ISEV

A quick pipeline for the isolation of 3D cell culture-derived extracellular vesicles

Heikki Kyykallio[1] | **Alessandra V. S. Faria**[2] | **Rosabella Hartmann**[2] | **Janne Capra**[1] | **Kirsi Rilla**[1] | **Pia R-M Siljander**[2]

[1]Institute of Biomedicine, University of Eastern Finland, Kuopio, Finland
(Email: janne.capra@uef.fi)

[2]EV Group, Molecular and Integrative Biosciences Research Programme, Faculty of Biological and Environmental Sciences, University of Helsinki, Helsinki, Finland

Correspondence
Dr. Rilla, Institute of Biomedicine, University of Eastern Finland, Kuopio, Finland.
Email: kirsi.rilla@uef.fi

Dr. Siljander, EV Group, Molecular and Integrative Biosciences Research Programme, Faculty of Biological and Environmental Sciences, University of Helsinki, Helsinki, Finland.
Email: pia.siljander@helsinki.fi

Funding information
Business Finland; Magnus Ehrnroothin Säätiö; Jane ja Aatos Erkon Säätiö; Mizutani Foundation for Glycoscience; Academy of Finland, Grant/Award Numbers: 330486, 337120, 337641

Abstract

Recent advances in cell biology research regarding extracellular vesicles have highlighted an increasing demand to obtain 3D cell culture-derived EVs, because they are considered to more accurately represent EVs obtained in *vivo*. However, there is still a grave need for efficient and tunable methodologies to isolate EVs from 3D cell cultures. Using nanofibrillar cellulose (NFC) scaffold as a 3D cell culture matrix, we developed a pipeline of two different approaches for EV isolation from cancer spheroids. A batch method was created for delivering high EV yield at the end of the culture period, and a harvesting method was created to enable time-dependent collection of EVs to combine EV profiling with spheroid development. Both these methods were easy to set up, quick to perform, and they provided a high EV yield. When compared to scaffold-free 3D spheroid cultures on ultra-low affinity plates, the NFC method resulted in similar EV production/cell, but the NFC method was scalable and easier to perform resulting in high EV yields. In summary, we introduce here an NFC-based, innovative pipeline for acquiring EVs from 3D cancer spheroids, which can be tailored to support the needs of variable EV research objectives.

KEYWORDS
3D cell culture, cancer spheroids, extracellular vesicles, isolation, nanofibrillar cellulose

1 | INTRODUCTION

Over the decades, cell culture has been applied as a major strategy for cell biology studies, especially in the cancer field, and various three-dimensional (3D) cell culture systems have emerged to better mimic in *vivo* conditions compared to traditional 2D cell cultures. Typically, most of the extracellular vesicle (EV) research has been conducted with cells grown in a monolayer on a dish to facilitate the isolation of EVs from the conditioned medium (Gudbergsson et al., 2016). However, the 2D cell cultures lack the impact of the extracellular matrix (ECM), which has been shown to dynamically affect multiple cellular processes such as proliferation, survival and energy metabolism (Jensen & Teng, 2020). Furthermore, cell polarity may be lost, and diversity of phenotypes diminished, because of the cell morphology in the 2D cell culture (Duval et al., 2017), and the limited cell-cell and cell-matrix contacts do not promote formation of environmental niches (Edmondson et al., 2014). In the 3D cell cultures, cells can become organized as in native tissues, and even form tissue-type features such as acinar structures of epithelium (Vidi et al., 2013) or importantly, cancer spheroids (Nath & Devi, 2016).

- -

Culture conditions in 2D vs 3D (or bioreactor) impact EV production, and both the yield of EVs and their cargo have been shown to be altered (Millan et al., 2021; Palviainen et al., 2019; Rocha et al., 2018; Thippabhotla et al., 2019; Villasante et al., 2021, Xie et al., 2017; Yang et al., 2020; Zhang et al., 2017). Critically in comparison to the EVs from monolayer cultures, 3D culture - derived EVs have been shown to be more akin to the EVs obtained from patients (Thippabhotla et al., 2019; Villasante et al., 2016). Currently, the lack of easy methods for obtaining EVs from 3D cell culture presents a bottleneck (Abdollahi, 2021). Both scaffold-free methods using ultra-low adhesion (ULA) plates (Sadovska et al., 2018), and biological scaffolds such as Matrigel, extracted from mouse sarcoma providing an in *vivo*-like ECM environment have been used for growing, for example, 3D cancer spheroids (Benton et al., 2014). Also, hydrogel scaffolds, composed of cross-linked polymeric material with high water content have been used, and they exhibit a tissue-like stiffness resembling natural ECM, but beneficially, they do not contain animal-derived molecular content (Caliari & Burdick, 2016). However, the gel-like structure of many 3D scaffolds and hydrogels is difficult to dissolve, which may prevent an efficient collection of EVs and cells for downstream analyses. Therefore, new 3D culture models for EV production and isolation are urgently needed.

A novel type of hydrogel can be obtained by using nanocellulose. The term nanocellulose covers cellulose-derived materials which in one dimension range into nanometre (Curvello et al., 2019). Wood-derived nanofibrillar cellulose (NFC) consists of long nanoscale fibres with a length of several micrometres, and it forms hydrogels already at low concentrations (0.1–0.2 wt.%) (Bhattacharya et al., 2012; Pääkkö et al., 2007). NFC exhibits similar viscoelastic properties with biological 3D scaffolds, diffusion of molecules, and biocompatibility for 3D culture with a number of human cell lines (Bhattacharya et al., 2012; Bicer et al., 2020; Malinen et al., 2014; Toivonen et al., 2016). Importantly, spheroid formation in NFC has already been well-characterized for varying cell types from ESC and iPSC (Lou et al., 2014) to human cancer cell lines such as HepaRG, HepG2 (Bhattacharya et al., 2012), MUG-Mel2 (Rinner et al., 2017), and urachal carcinoma (Mäkelä et al., 2020). As detailed in Azoidis et al. (2017), mesenchymal stem cells (MSC) embedded in 0.2% NFC were seen to form spheroids which were isotropically and homogenously distributed throughout the hydrogel and were found to be equally metabolically active and proliferate at a rate equal to MSC grown in 2D (Azoidis et al., 2017). Spheroid formation and increasing spheroid diameter were shown during culture of undifferentiated and differentiated HepaRG cells through 14 days of culture in NFC (Malinen et al., 2014). NFC can be digested into soluble glucose with cellulases, allowing cell/spheroid retrieval from the culture (Lou et al., 2014). From the EV point of view, the lack of animal-derived molecules and EVs that may contaminate biological scaffolds, and the efficient digestion of the hydrogel make NFC a promising matrix for 3D cancer spheroid-derived EV production and isolation.

In this technical report, we introduce a quick NFC-based pipeline consisting of two methods for the isolation of EVs to enable different study strategies: a batch method as an endpoint to isolate all EVs after digestion of the NFC, and a harvesting method to enable successive, time-wise combination of EV production with the monitoring of spheroid growth and properties, which can be reproduced and adapted for different human cell lines and EV isolation methods.

2 | MATERIALS AND METHODS

2.1 | Cell lines

A2058 melanoma cell line was kindly donated by Dr. Pasonen-Seppänen (University of Eastern Finland) and cell line authentication was made by Genotyping Unit, Technology Centre Institute for Molecular Medicine Finland FIMM, University of Helsinki. The creation of MCF7 human breast cancer cell line with stable doxycycline-inducible green fluorescent protein-hyaluronan synthase 3 (GFP-HAS3) expression was described in (Siiskonen et al., 2013). For this study, the inducible GFP-HAS3 protein on the cell plasma membrane and EVs enabled visualization of the live spheroids and secreted EVs. GFP-HAS3 induction was not used in experiments where EVs were isolated.

2.2 | 2D cell culture

2.2.1 | Melanoma

A2058 cell line was cultured in routine cell culture medium [Dulbecco modification of Minimum Essential Media (Sigma-Aldrich, Media Kitchen, University of Helsinki) supplemented with 10% fetal bovine serum (FBS) (Gibco, Thermo Fischer Scientific, USA), 1% penicillin-streptomycin (5.000 U/ml – Thermo Fischer Scientific)]. Cells were passaged twice a week using 3.5×10^4 cells/cm^2 split ratio using 0.05% trypsin (w/v) (Media Kitchen, University of Helsinki) with 0.02% EDTA (w/v) (Avantor Inc., USA). Cells were counted by trypan blue dye exclusion, and the optimal viability was considered to be 95%–97%. In all experiments in which A2058 cells were used, the passage number was not higher than 20.

2.2.2 | Breast cancer

MCF7-GFP-HAS3 cell line was cultured in routine cell culture medium [minimum essential medium alpha (MEMα, Euro-Clone, Italy) supplemented with 5% FBS (Gibco, Thermo Fischer Scientific, USA), 2 mM glutamine (EuroClone, Italy), 50 μg/ml streptomycin sulphate and 50 U/ml penicillin (BioWhittaker, Lonza, Switzerland) and maintained with 50 μg/ml hygromycin B (Invitrogen)]. Cells were passaged twice a week with a 1:5 split ratio using 0.05% trypsin (w/v) 0.02% EDTA (w/v) (Biochrom AG, Germany), and the optimal cell viability was considered to be 94%–96%. In all experiments in which MCF7 cells were used, the passage number was not higher than 22.

2.3 | Protocols for generating EV-depleted FBS

FBS (Gibco) was depleted from EVs using ultracentrifugation (for breast cancer cell MCF7 experiments) or polyethylene glycol (PEG 10000) (for melanoma cell A2058 experiments). Shortly, the EV-depleted FBS was prepared by ultracentrifugation at 110,000 $\times g$ for 16 h. After centrifugation, the supernatant was collected and sterile-filtered (0.22 μm). A PEG 10000 (Sigma-Aldrich, USA) 50% (w/v) stock solution was prepared in Dulbecco's phosphate buffered saline (dPBS) [sterile filtered (0.2 μm)]. The PEG stock solution was stored protected from light and at 4°C. The FBS and PEG stock solution were mixed in a 5:1 ratio by gently inverting 5–10 times and incubated for 2 h at 4°C protected from light. After, the mix of PEG-FBS was centrifugated for 30 min at 4°C at 1500 $\times g$ in a swinging-bucket rotor (four place, angle 90°, Hettich, Germany) in benchtop centrifuge (Rotina 380, Hettich, Germany). The supernatant of the PEG-FBS solution was collected leaving a layer of at least 0.5 cm on top of the pellet, and again sterile filtered (0.1 μm) into aliquots stored at –20°C until used (Laukkanen et al., 2020).

2.4 | 3D culture for batch method isolation

To prepare poly(2-hydroxyethyl methacrylate) (Poly-HEMA)-coated plates, 1.2% (w/v) Poly-HEMA (Sigma-Aldrich, USA) was dissolved into 95% EtOH overnight at 65°C and filtered with 0.22 μm filter (Guangzhou Jet Biofil, China). To coat the wells of a 48-well plate (Cellstar, Greiner Bio-one, Austria), 70 μl of 1.2% Poly-HEMA solution was added per well. The solution was allowed to evaporate overnight, and coating was repeated the next day. Before use, the wells were washed three times with dPBS (Corning, USA). For the 3D spheroid culture, 1.5% (w/v) GrowDex® NFC hydrogel (UPM Biomedicals, Finland) was diluted with experiment medium [minimum essential medium alpha (MEMα, EuroClone, Italy) supplemented with 5% UC-EV-depleted FBS, 2 mM glutamine (EuroClone, Italy), 50 μg/ml streptomycin sulphate and 50 U/ml penicillin (BioWhittaker, Lonza, Switzerland)] into 0.5% (w/v) working concentration. Next, 250,000 cells* were suspended into 1 ml of the prepared NFC-scaffold and 300 μl of the NFC-cell mixture was added per well. Experiment medium [minimum essential medium alpha (MEMα, Euro-Clone, Italy) supplemented with 5% UC-EV-depleted FBS, 2 mM glutamine (EuroClone, Italy), 50 μg/ml streptomycin sulfate and 50 U/ml penicillin (BioWhittaker, Lonza, Switzerland)] (300 μl) was then added on top of the hydrogel. Cultures were grown at 37°C, 5% CO$_2$ for 7 days to allow formation of spheroids. The medium on top of the hydrogel was refreshed twice by aspirating 150 μl of conditioned medium and adding 150 μl of fresh experiment medium [minimum essential medium alpha (MEMα, Euro-Clone, Italy) supplemented with 5% UC-EV-depleted FBS, 2 mM glutamine (EuroClone, Italy), 50 μg/mL streptomycin sulphate and 50 U/ml penicillin (BioWhittaker, Lonza, Switzerland) on days 2 and 5 during the experiment. For induction of GFP-HAS3 expression, 1 μg/ml doxycycline (doxycycline hydrochloride, Sigma-Aldrich) was added with each medium change. *For each cell line optimal growth time and cell number needs to be determined. As a starting point, the GrowDex® manufacturer UPM can provide NFC-growth information for >200 different commonly used cell lines.

2.5 | 3D culture using NFC for harvesting method

For the harvesting method, 1.5% (w/v) GrowDex® NFC hydrogel or 1% (w/v) GrowDex®-T anionic NFC hydrogel (aNFC) (UPM Biomedicals, Finland) was diluted with experiment medium [Dulbecco modification of Minimum Essential Media (Sigma-Aldrich, Media Kitchen, University of Helsinki) supplemented with 10% PEG-EV-depleted FBS, 1% penicillin-streptomycin (5.000 U/ml – Thermo Fischer Scientific)] into working concentration 0.5% (w/v). After preparation of the NFC/aNFC scaf-folds, 25,000 cells were mixed with NFC/aNFC (final concentration 0.5%) and 300 μl of the mixture was added per well on a 48-well plate (ThermoFisher Scientific, USA). Two different protocols were used: (i) refreshed medium and (ii) top-up of medium. For refresh medium protocol, every two days the content of the well was centrifuged at 1000 $\times g$ for 10 min, the super-natant was collected for EV isolation, and followed the steps: centrifugation at 1000 $\times g$ (Fresco™ 21 Microcentrifuge, Thermo Scientific, USA; 24 $\times$ 1.5/2.0 ml Rotor with ClickSeal™ Biocontainment Lid Fixed angle (45°), Thermo Scientific, USA) for 10 min. The supernatant was collected for EV isolation, and the sedimented NFC/aNFC-scaffold containing the cells was mixed with

fresh experiment medium [Dulbecco modification of Minimum Essential Media (Sigma-Aldrich, Media Kitchen, University of Helsinki) supplemented with 10% PEG-EV-depleted FBS, 1% penicillin-streptomycin (5.000 U/ml – Thermo Fischer Scientific)] and re-seeded on a new 48-well plate. For top-up medium protocol, 50 μl of fresh experiment medium [Dulbecco modification of Minimum Essential Media (Sigma-Aldrich, Media Kitchen, University of Helsinki) supplemented with 10% PEG-EV-depleted FBS, 1% penicillin-streptomycin (5.000 U/ml – Thermo Fischer Scientific)] was added every 2 days on top of the spheroids, and the conditioned medium and spheroids were collected at day 11. At the endpoint of each experiment, the pellet was collected and digested with 600 $\mu g/mg$ (μg enzyme/mg cellulose) GrowDase™ cellulase enzyme mix (UPM Biomedicals, Finland) by incubating in 37°C, 5% CO_2 for 24 h to recover the spheroids. After digestion, the spheroids were either (i) suspended into 0.5 ml of 0.05% trypsin and incubated in 37°C for ~25 min until the cells were detached, and cells were counted by trypan blue exclusion, or (ii) spheroids were lysed for measuring protein concentration.

2.6 | 3D culture using ULA plates for comparison with the harvesting method

For the 3D culture using ultra-low-attachment (ULA) Nuclon™ Sphera™ 96-Well, Nuclon Sphera-Treated, U-Shaped-Bottom Microplate (ThermoFisher Scientific, USA), A2058 cells were seeded at 2500 cells/well with experiment medium [Dulbecco modification of Minimum Essential Media (Sigma-Aldrich, Media Kitchen, University of Helsinki) supplemented with 10% PEG-EV-depleted FBS, 1% penicillin-streptomycin (5.000 U/ml – Thermo Fischer Scientific)], and the plate was centrifuged at 300 × g, 5 min, and the plate was incubated at 37°C, 5% CO_2, humidified atmosphere, for 24 h to enable spheroid formation. The conditioned medium was harvested from 10 ULA wells, pooled together, and compared with the medium from one well of NFC grown cells. Two different protocols were used: (i) refreshed medium and (ii) top-up of medium. For refresh medium protocol, every two days the content of the well was centrifuged at 1000 × g for 10 min and the supernatant was collected for EV isolation. The spheroids were re-seeded into ULA plates with fresh experiment medium [Dulbecco modification of Minimum Essential Media (Sigma-Aldrich, Media Kitchen, University of Helsinki) supplemented with 10% PEG-EV-depleted FBS, 1% penicillin-streptomycin (5.000 U/ml – Thermo Fischer Scientific)] in each well. For top-up medium protocol, 25 μl of fresh experiment medium [Dulbecco modification of Minimum Essential Media (Sigma-Aldrich, Media Kitchen, University of Helsinki) supplemented with 10% PEG-EV-depleted FBS, 1% penicillin-streptomycin (5.000 U/ml – Thermo Fischer Scientific)] was added every 2 days on top of the spheroids, and the conditioned medium and spheroids were collected at day 11.

2.7 | EV isolation for batch method

After a 7-day culture period, NFC scaffold of the breast cancer spheroid cultures was digested with 600 $\mu g/mg$ (μg enzyme/mg cellulose) GrowDase™ cellulase enzyme (UPM Biomedicals, Finland) by incubating in 37°C, 5% CO_2 for 9–24 h (specified in results). After digestion, the remaining culture medium from three wells was pooled together and centrifuged at 600 × g for 10 min to pellet the spheroids, and the supernatant containing the EVs was collected. To calculate the number of cells from spheroids, the spheroid pellet was suspended into 0.5 ml of 0.05% trypsin and incubated in 37°C for ~15 min until the cells were detached. The collected supernatant was centrifuged at 5000 × g for 15 min at 4°C to remove cell debris and possible non-digested cellulose fibres and the pellet was discarded. The optional filtering step was performed with Minisart 5.0 μm syringe filters (Sartorius, Germany). EVs were isolated by ultracentrifugation at 189,000 × g for 90 min at 4°C (Beckman Optima L-90K ultracentrifuge with Beckman Type 50.4 Ti fixed-angle rotor, adjusted k-factor 88, Beckman Coulter, USA). After centrifugation, the pellets were suspended into dPBS which had been sterile filtered with 0.22 μm syringe filters.

2.8 | EV isolation for harvesting method

For EV isolation, the following protocol was applied for all the conditioned media. The medium was centrifuged at 5000 × g for 30 min at 4°C and the pellet, containing debris, was discarded. The EVs were isolated from the supernatant by ultracentrifugation at 110,000 × g (Optima MAX XP Ultracentrifuge – TLA55 Fixed-Angle 45° Rotor, k-Factor 66, Beckman Coulter, USA) for 120 min at 4°C, as described before (Palviainen et al., 2020). After discarding the supernatant, the pellet was suspended in dPBS (Sigma Aldrich, USA). The size and concentration of fresh EVs were measured by Malvern NTA, and the spare EVs were stored at −80°C.

2.9 | Spheroid protein extraction and concentration

Protein extraction and concentration measurement were performed as described before (Faria et al., 2020). Briefly, cells were lysed for 2 h on ice in cell lysis buffer (50 mM Tris–HCl pH 7.4, 1% Tween 20, 0.25% sodium deoxycholate, 150 mM NaCl, 1 mM ethylene glycol-bis(β-aminoethyl ether)-N,N,N',N'-tetraacetic acid (EGTA), 1 mM Na_3VO_4, 1 mM NaF, and protease inhibitors [1 μg/mL aprotinin, 10 μg/ml leupeptin, and 1 mM 4-(2-aminoethyl) benzenesulfonyl-fluorid-hydrochloride]. Protein extracts were cleared by centrifugation and protein concentration was determined using the Lowry reagent (BioRad, USA).

2.10 | SDS-PAGE and Western blot

Western blot was performed as described before (Palviainen et al., 2020). Briefly, 1.5×10^{10} particles (measured by nanoparticle tracking analysis) of cell-derived EVs were lysed in 2× Laemmli buffer (100 mM Tris-HCl [pH 6.8], 200 mM dithiothreitol, 4% SDS, 0.1% bromophenol blue and 20% glycerol) and samples were boiled for 10 min. EVs extracts were resolved by 12% SDS-PAGE (sodium dodecyl sulphate-polyacrylamide gel electrophoresis) for 1.5 h and transferred to polyvinylidene difluoride (PVDF) membranes using Trans-Blot Turbo Transfer System [25 V, 0.5A, 25 min] (BioRad Laboratories, USA). Membranes were blocked in 5% BSA in TBS-T (TBS with 0.5% Tween 20), and then incubated with antibodies 1:1000 (BSA 1% diluted TBS with 0.5% Tween 20) against human CD9 (Santa Cruz, sc13118), and Calnexin (Cell Signaling Technology, #2679). Proteins of interest were detected with 1:5000 (BSA 1% diluted TBS with 0.5% Tween 20) diluted HRP-conjugated IgG antibody (NA931 anti-mouse HRP, and NA934 anti-rabbit HRP, GE Healthcare, USA) and visualized with the Clarity ECL substrate (BioRad Laboratories, USA) using the ChemiDoc Imaging Systems (BioRad Laboratories, USA).

SDS-page staining with Coomassie Blue was performed after the gel running step with 25 ml Coomassie Blue (0.1% Coomassie Blue R250, 50% methanol, 10% acetic acid, 40% water for 5 min. After, the excess of Coomassie Blue staining was removed with 50 ml destaining solution (50% methanol, 10% acetic acid, 40% water for 3 h.

2.11 | Nanoparticle tracking analysis

Particle concentration and size distribution of the isolated MCF7-EV samples were determined by nanoparticle tracking analyser (NTA) (Malvern Instruments Ltd. Malvern, UK) with an NS300 view unit. Four measurements were performed with the following settings for data acquisition: camera level 13, acquisition time 30 s and detection threshold 3. NTA 3.1 Software (Nanosight, UK) was used for the analysis.

NTA of A2058 EVs was performed as described previously (Palviainen et al., 2020). Briefly, LM14C (NanoSight Ltd., UK) equipped with blue (404 nm, 70 mW) laser and sCMOS camera were used. Settings for data acquisition were: camera level 14, SOP Standard Measurement, auto-settings off, polydispersity medium, reproducibility high, and acquisition time 5 × 30 s. The sample was diluted into 0.1 μm filtered buffer pre-checked for the absence of particles. Each sample was diluted to an optimal 40–100 particles/frame concentration for measurement. Data were analysed with NanoSight NTA 3.0 software with the following settings: auto background subtraction/blur/minimum track length, and detection threshold 5.

2.12 | Scanning electron microscopy and transmission electron microscopy

For scanning electron microscopy of isolated EVs and empty NFC isolates, 13 mm cover glasses were coated with Poly-D-Lysine (Sigma-Aldrich) overnight and washed 3 times with PBS. EV- and empty NFC preparations were added on the cover glasses and incubated at 4°C overnight. The preparations were fixed with 2% glutaraldehyde and 1% osmium tetroxide and dehydrated in ascending series of ethanol before drying with hexamethyldisilazane and coating with chromium. Imaging was performed using a Carl Zeiss Sigma HD VP scanning electron microscope (Carl Zeiss NTS, UK) operated at 5 kV.

For transmission electron microscopy: negative staining was performed as previously described (Puhka et al., 2017; Palviainen et al., 2019). Briefly, EVs were loaded on 200 mesh grids without dilution, were fixed with 2.0 % PFA in $NaPO_4$ buffer, stained with 2% neutral uranyl acetate, further stained and embedded in uranyl acetate and methyl cellulose mixture (1.8/0.4%). Stained samples were viewed with transmission electron microscopy using Jeol JEM-1400 (Jeol Ltd., Tokyo, Japan) operating at 80 kV. Images were taken with Gatan Orius SC 1000B CCD-camera (Gatan Inc., USA) with 4008 × 2672 px image size and no binning.

2.13 | Single particle interferometric reflectance imaging sensor (SP-IRIS)

The SP-IRIS ExoView® R100 protocol was followed as indicated by manufacturer (NanoView Biosciences, USA). Briefly, the samples from days 3, 5, 7, 9, and 11 from aNFC harvesting method, day 7 from batch method, and day 11 from ULA plate were thawed out and centrifuged 2500 × g (MIKRO 200R centrifuge, fixed angle rotor [45°] 24-places), 15 min, 19°C. Next, the samples

were diluted 1:1 in solution B from the manufacturer and incubated on the ExoView Tetraspanin Chip (EV-TETRAC) placed in a sealed 24-well plate for 16 h at room temperature. The chips were then washed three times in one mL solution A for three min each on an orbital shaker. Then, chips were incubated with ExoView Tetraspanin Labelling Abs that consist anti-CD81 Alexa-555, anti-CD63 Alexa-647, and anti-CD9 Alexa-488. The antibodies were diluted 1:500 in blocking buffer (provided by company NanoView Biosciences, USA). The chips were incubated with 250 μl of the labelling solution for 1 h and washed once in solution A, three times in solution B followed by a rinse in filtered milliQ water and dried. The chips were then imaged with the ExoView R100 reader using the ExoScan 3.0 acquisition software. The data were analysed using ExoViewer 2.5.0 with sizing thresholds set from 50 to 200 nm diameter, and the dilution factor was calculated and normalized by particle concentration (from Malvern NTA). The antibodies, solutions A, B, and blocking buffer were provided by the manufacturer.

2.14 | Spheroid growth and viability in NFC and aNFC

Phase contrast images of spheroids were obtained by EVOS XL Core Cell Imaging System (ThermoFischer Scientific, USA). Spheroid morphology was followed up by microscopy (20× or 40× magnification). Size of the spheroids was measured using Fiji software as described in (Schindelin et al., 2012). The viability of the A2058 spheroids in NFC and aNFC during harvesting method was followed every 2 days (from days 3–11). Following the harvesting method protocol, the cell cultures were collected and centrifuged $1000 \times g$ for 10 min (Hettich Mikro 20 centrifuge). The NFC/aNFC pellet containing the spheroids was resuspended with fresh medium and 100 μl of the resuspended culture was added on a 16-well chamber slide (Culturewell™ chamberSLIP 16, Grace Bio-Labs, Bend, OR, USA). Prior to imaging, the nuclei of the spheroids were stained with NucBlue® Live ReadyProbes® Reagent (Life Technologies, USA) according to manufacturer's protocol and with 0.06 mM propidium iodide (Santa Cruz) to visualize dead cells. The wells were washed once with PBS and the live spheroids were immediately imaged. For MCF7 day 7, and A2058 day 11 top-up cultures, the culture medium was aspirated and 100 μl of the NFC/aNFC spheroid culture was transferred to a 16-well chamber slide per well and stained as previously before imaging. The live/dead cell ratio was calculated by counting the total number of nuclei, and the number of dead nuclei from the confocal images using ImageJ software (National Institute of Health, Bethesda, MD, USA). A total of 136–766 nuclei were counted per day/cell line.

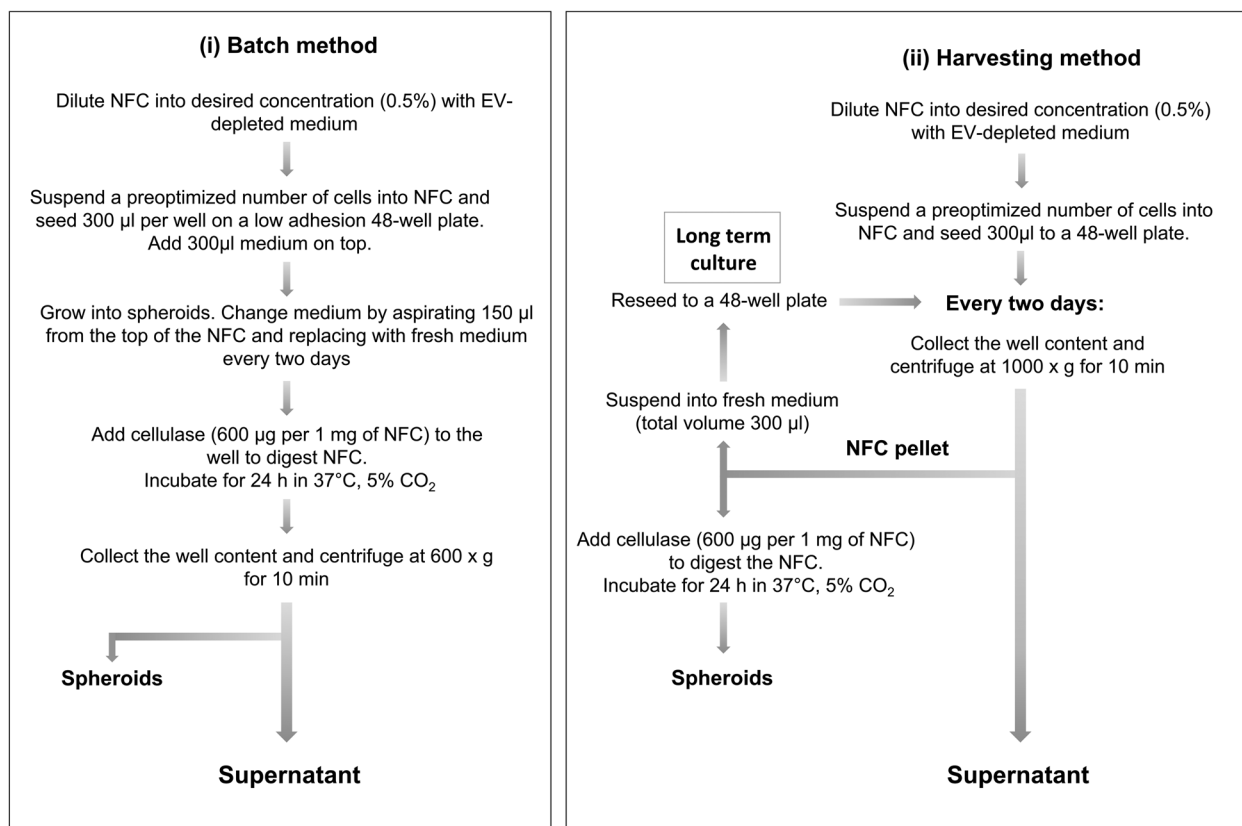## 2.15 | Live-cell confocal microscopy and image processing

Confocal imaging of spheroid cultures was performed with Zeiss Axio Observer microscope, with 20 × NA 0.8 and 63 × NA 1.4 oil objectives, equipped with LSM800 confocal module (Carl Zeiss Microimaging GmbH, Jena, Germany). ZEN v2.5 Blue software (Carl Zeiss Microimaging GmbH) and ImageJ were utilized for image processing and 3D rendering.

2.16 | Proliferation and morphology assay

HEK293 cells were routinely grown in Dulbecco modification of Minimum Essential Media (Sigma-Aldrich, Media Kitchen, University of Helsinki) supplemented with 10% FBS, 1% penicillin-streptomycin (5.000 U/ml – Thermo Fischer Scientific). For proliferation and morphology assay, HEK293 were cultured in experiment medium [Dulbecco modification of Minimum Essential Media (Sigma-Aldrich, Media Kitchen, University of Helsinki) supplemented with 10% PEG-EV-depleted FBS, 1% penicillin-streptomycin (5.000 U/ml – Thermo Fischer Scientific)]. HEK293 were seeded into 96-well plates, at a density of 5×10^4 cells/well, and treated with A2058 NFC EVs from batch and harvesting methods (1×10^9 EVs/mL by NTA – concentration based on Pacienza et al., 2018 and Nguyen et al., 2020); no-EVs addition and only cellulase [600 μg/mg (μg enzyme/mg cellulose) GrowDaseTM cellulase enzyme (UPM Biomedicals, Finland)] were used as controls. After 24 h, the medium was removed, and cells were washed three times with PBS, and fixed with PFA (4% in PBS) for 10 min. Next, cells were permeabilized with Triton-X100 (0.1% in PBS) for 10 min. Cells were stained with Hoechst 34580 (ThermoFisher Scientific) and Actin red (ActinRed™ 555 ReadyProbes™ Reagent (Rhodamine phalloidin), ThermoFisher Scientific), diluted 1:5000 in PBS, for 30 min. Cells were washed three times with PBS and images were obtained by EVOS XL Core Cell Imaging System (ThermoFischer Scientific), using 10× and 20× magnification. The live cell number was calculated by counting the total number of nuclei from the images using ImageJ software (National Institute of Health, Bethesda, MD, USA).

2.17 | Statistical analysis

Statistical analyses were performed using GraphPad Prism Software v.5.00 for Windows, (GraphPad, USA), and R program (R Core Team 2013)). Two-way ANOVA with Tukey's post-hoc test was calculated, and (*) $P < 0.05$, (**) $P < 0.01$, (***) $P < 0.001$

(i) Batch method

Dilute NFC into desired concentration (0.5%) with EV-depleted medium

Suspend a preoptimized number of cells into NFC and seed 300 µl per well on a low adhesion 48-well plate. Add 300µl medium on top.

Grow into spheroids. Change medium by aspirating 150 µl from the top of the NFC and replacing with fresh medium every two days

Add cellulase (600 µg per 1 mg of NFC) to the well to digest NFC. Incubate for 24 h in 37°C, 5% CO_2

Collect the well content and centrifuge at 600 x g for 10 min

Spheroids

Supernatant

(ii) Harvesting method

Dilute NFC into desired concentration (0.5%) with EV-depleted medium

Suspend a preoptimized number of cells into NFC and seed 300µl to a 48-well plate.

Long term culture

Reseed to a 48-well plate

Every two days:

Collect the well content and centrifuge at 1000 x g for 10 min

Suspend into fresh medium (total volume 300 µl)

NFC pellet

Add cellulase (600 µg per 1 mg of NFC) to digest the NFC. Incubate for 24 h in 37°C, 5% CO_2

Spheroids

Supernatant

3D cell culture EVs ready for isolation and characterization

FIGURE 1 Flowchart for batch and harvesting methods to isolate EVs from NFC 3D cultures. For the batch method (i) the NFC is first diluted to the desired NFC concentration (depends on the cell type), a preoptimized number of cells are suspended into the NFC and 300 μl of the suspension is seeded on a 48-well plate. Medium (300 μl) is added on top of the hydrogel, and the cells are allowed to grow into spheroids with the medium changed every two days by carefully aspirating 150 μl of the medium from top of the NFC and gently adding 150 μl of medium. To release the spheroids and EVs trapped in the NFC, 600 μg of cellulase per mg of NFC is diluted with medium to 300 μl and the mixture is added in the culture well and incubated for 24 h in +37°C. The spheroids are removed by centrifugation at 600 × g for 10 min and the supernatant is collected for EV isolation. To remove cell and NFC debris, the supernatant is first centrifuged at 5000 × g for 15 min at 4°C and the pellet is discarded. The supernatant can then be filtered to increase sample purity. EVs are finally isolated with a method of choice, for example in this case ultracentrifugation at 189,000 × g for 90 min at 4°C. The pellet containing the EV is suspended into PBS. For the harvesting method (ii) both the NFC dilution and cell seeding are done similarly as in the batch method, but the well content is collected every two days and centrifuged at 1000 × g for 10 min. The supernatant is collected and centrifuged at 5000 × g for 30 min at 4°C to remove cell and NFC debris and the pellet is discarded. EVs are isolated from the supernatant with a method of choice, for example, in this case by ultracentrifugation at 110,000 × g for 120 min at 4°C and the pellet containing the EV is suspended into PBS. The NFC pellet from cell cultures is resuspended into fresh conditioned medium (300 μl) and reseeded back to a 48 well plate to continue the culture, or it can be digested with 600 μg of cellulase per mg of NFC (diluted with medium to 300 μl) for 24 h to release the spheroids

was considered significant. Experiments were performed in biological replicates and each data is shown by dot plot graphic together with a boxplot.

3 | RESULTS

3.1 | 3D spheroid culture in NFC and EV isolation

To establish a novel pipeline for 3D EV isolation, NFC hydrogel was utilized as a scaffold for growing cancer spheroids. 3D spheroid cultures of MCF7 breast cancer and A2058 melanoma cell lines were established in NFC and optimized into two separate workflows for the isolation of EVs from the 3D cultures (detailed flow charts are given in Figure 1). To isolate spheroids and the secreted EVs from the matrix, two methods were developed regarding NFC digestion: with (batch) or without (harvesting)
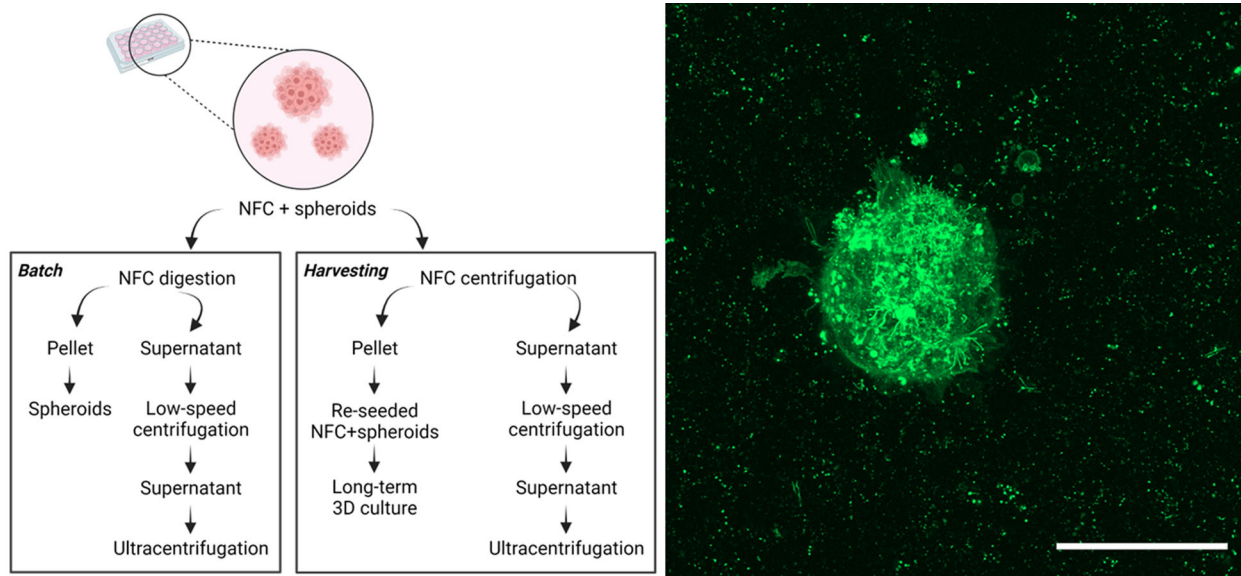
FIGURE 2 Quick pipeline for EV isolation from NFC-cultured 3D spheroids – batch and harvesting method. Briefly, the cancer spheroids were cultured in NFC, and the EV –containing conditioned medium was accessed by (i) NFC digestion with cellulase, aiming for maximal recovery of EVs (**batch method**); (ii) removing the NFC & spheroid mixture and separating the conditioned medium for EV isolation and subsequently re-plating the mix of NFC & spheroids every two days for long-term 3D culture (**harvesting method**). Confocal 3D maximum intensity projection of a live MCF7 spheroid expressing GFP-HAS3 grown in NFC is shown in the right panel. Scale bar: 50 μm. Figure (flow chart) created with Biorender.com

cellulase, which breaks up NFC into soluble glucose without disturbing the cells and cellular structures. The aim of the batch method was to maximize the EV recovery by breaking down all NFC networks to release the highest amount of EVs possible. The harvesting method was created to support time-wise EV isolation enabling long-term 3D spheroid culture (re-utilizing the mix of NFC & spheroids) and monitoring. Both methods are summarized in Figure 2 and described in detail under the following topics.

3.1.1 | Spheroid viability in NFC

Although the NFC is already a well-established matrix and shown to support growth of different cell lines, cell viability is an important factor that facilitates the secretion of EVs, especially apoptotic bodies. To ensure the viability of spheroids during both batch and harvesting methods, the growth and viability of the MCF7 and A2058 cells in NFC and anionic, optically transparent aNFC were followed by phase contrast and confocal microscopy (Supplementary Figure 1). Both cell lines formed spheroids with distinct morphologies: A2058 cells formed less organized grape-like structures, while MCF7 spheroids were spherical. Typical lumen-like structures for MCF7 cells were also observed after 7 days in culture.

The viability of spheroids for the batch and harvesting methods was confirmed for the time-points utilized for the EV isolation (Supplementary Table 1). For the MCF7 spheroids (batch method), the viability of the cells in spheroids was 93% on day 7. For the A2058 spheroids (harvesting method), the spheroid viability was followed every two days after the 1000 x g centrifugation and resuspension of the culture. In NFC, the viability was between 91% and 94% on days 5–11. Without the centrifugation step the viability of cells was 88 % on day 11. In aNFC the viability was 89%–91% when spheroids were centrifuged and 87 % without the centrifugation on day 11. The morphology of the spheroids also remained similar, implying that the centrifugation and resuspension did not alter the spheroid structure. Additionally, no necrotic core formation was observed in spheroids from either cell line.

3.2 | Optimization of EV isolation protocol by the batch method

For the batch method, MCF7 breast cancer cells were grown in 0.5% NFC for 7 days to allow formation of spheroids. The NFC scaffold was then digested with cellulase to release the spheroids and EVs trapped in the scaffold (Figure 2). To isolate the EVs from the culture medium for characterization, we optimized the NFC digestion and isolation protocol for differential centrifugation.

First, the NFC concentration (Figure 3A) and digestion time (Figure 3B) were optimized to minimize the number of NFC-derived contaminant particles in the EV isolates. Empty NFC scaffolds (no cells) with concentrations of 0.5%, 0.7% and 0.9%
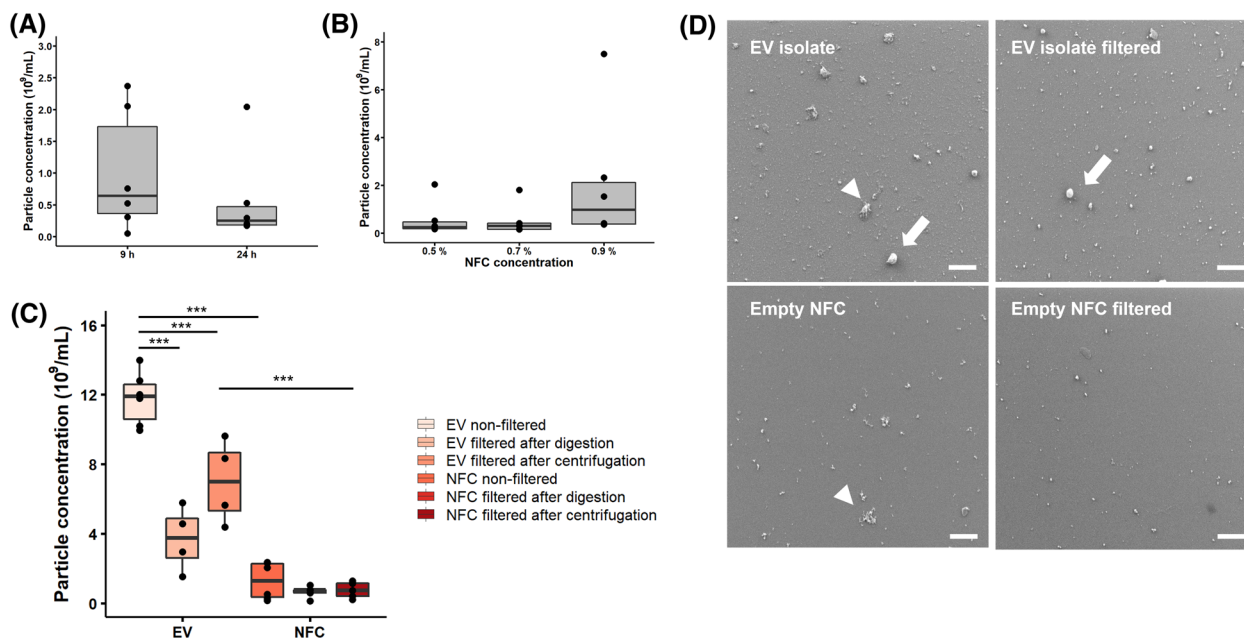
FIGURE 3 Effect of NFC concentration, cellulase digestion time, and supernatant filtering on sample purity and particle concentration by NTA. (A) High concentration of NFC increased the number of particles and variation of particle concentrations from the empty NFC scaffolds, $n = 6$ independent experiments. *T*-test, (n.s.). (B) Increasing the time of cellulase digestion decreased the number of empty NFC derived particles, n = 6 independent experiments. One-way ANOVA with Tukey's post hoc test, (n.s.). (C) Comparison of particle concentrations from the cell culture (EV) and empty NFC (NFC) samples with different filtering steps, n = 4-6 independent experiments. One-way ANOVA with Tukey's post hoc test, *** $P < 0.001$. (D) The non-filtered and filtered samples were compared with scanning electron microscopy. Cell culture samples contained a high number of spherical particles of variable sizes with vesicle-like morphology (arrows). Fibre-like structures found in the non-filtered samples (arrowheads) were absent in the filtered samples. Scale bars:1 μm

NFC (w/v) were digested, and the medium was centrifuged as described by the EV isolation protocol. Only a small number of particles within size range comparable to EVs was detected in the empty NFC digestions (Supplementary Figure 2) and the number increased with 0.9% NFC (Figure 3A). Thus, the 0.5% NFC concentration was selected for further isolations, as it also gave a good yield of EVs, as detected by NTA. Next, we proceeded to investigate whether the recommended 24 h digestion time could be significantly reduced to 9 h without increasing the NFC scaffold-derived impurities in the samples. Samples from empty NFC scaffolds from the two time points were digested, centrifuged, and measured with NTA (Figure 3B). Since a trend in reduction of particle numbers was observed, we recommend a longer incubation period to ensure higher purity of the EV samples.

To further improve the purity of EVs isolated by cellulose digestion in the batch method, an additional filtration step was tested by comparing it with centrifugation only. For this, the MCF7 spheroids were grown for 7 days in 0.5% NFC and the NFC was digested for 24 h to recover the maximum number of EVs from the conditioned matrix. Filtering the samples immediately after the removal of spheroids reduced the concentration of empty NFC-derived impurities (n.s.), but the concentration of particles (EVs) from the cell culture samples was significantly reduced (Figure 3C). Centrifugation (5000 $\times g$) followed by filtration (5 μm) before the isolation of EVs by ultracentrifugation decreased the presence of empty NFC derived particles with a similar trend, and the concentration of cell culture derived particles (EVs) was again reduced, although slightly less than with the earlier filtering, on average (Figure 3C). EV yield without filtering was $1.18 \times 10^{10} \pm 1.54 \times 10^{9}$ particles/ml, with filtering directly after digestion $3.71 \times 10^{9} \pm 1.86 \times 10^{9}$ particles/ml and with filtering after the 5000 $\times$ g centrifugation $7.00 \times 10^{9} \pm 2.40 \times 10^{9}$ particles/ml.

The non-filtered and filtered samples from MCF7 spheroids as well as the non-filtered and filtered samples from empty NFC scaffolds were analysed with scanning electron microscopy (Figure 3). The EV isolates from MCF7 spheroids contained a high number of heterogeneously sized particles, most of which had a round vesicle-like morphology (arrows in Figure 3). The occasional fibre-like, bigger particles found in the non-filtered cell-culture-derived and empty NFC samples (Figure 3, arrowheads) were absent in the filtered samples.

3.3 | Harvesting method

To avoid the need for NFC digestion and to directly recover EVs, a second method was developed, which also enables monitoring time-wise changes in the EV production and tying these changes into distinct phases during the spheroid growth (Figure 2). For this harvesting method, the conditioned medium was collected every two days followed by low-speed centrifugation at 1000 $\times g$

TABLE 1 Protein concentration and number of cells from spheroids grown in NFC (day 11)

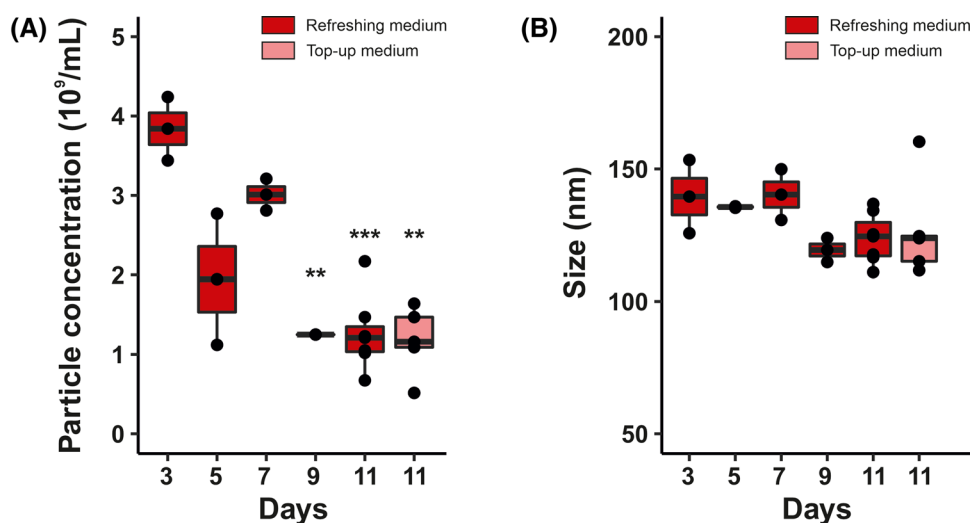| Culture condition	Protein concentration ($\mu g/\mu l$)	Number of cells ($\times 10^5$)
Refreshing medium	13.0 ± 0.7	1.8 ± 0.9
Top-up	13.2 ± 0.1	2.2 ± 0.6

FIGURE 4 **Concentration of EVs obtained by the harvesting method**. Comparison of the effect of i) refreshing the medium completely and ii) topping up with the fresh medium on particle numbers by NTA. (A-B) To compare the refreshing with topping up, A2058 cells were seeded in NFC, and the conditioned medium was harvested for EV isolation, and particle concentration (A) and particle size (B) were measured by NTA from 3 to 6 independent experiments Statistics: ANOVA with Tukey's post-hoc test. Day 3 vs Day 9, Day 3 vs Day 11 top-up medium: (**) $P < 0.01$, Day 3 vs Day 11 refreshing medium: (***) $P < 0.001$

for 10 min – this centrifugation did not destroy the NFC or the spheroids and allowed the EV-rich supernatant to be collected for EV isolation. The remaining pellet (NFC & spheroids) was re-seeded into wells to continue the culturing by gently resuspending fresh medium on the NFC. We tested the effect of two cell culturing routines on EV recovery: refreshing the medium every two days as described, and only topping up fresh medium every two days. Protein concentration and number of cells (Table 1) were similar between the methods showing no impact on spheroid growth. According to NTA, the particle concentrations dropped over time, and the best EV production was found on day 3 (Figure 4). Also, here the potential contamination of NFC-derived particles was analysed by incubating empty NFC + cell culture medium at the same condition as the spheroids. The number of particles derived from empty NFC was lower than 10% of the concentration obtained from day 3, (NFC + culture medium: 3.8×10^{10} particles/ml, empty NFC 0.2×10^{10} particles/ml) – (NTA size-distribution graphics: Supplementary Figure 4).

3.3.1 | Parallel comparison of the EV production with A2058 spheroid growth using the harvesting method

Since the harvesting method enables time-wise acquisition of EVs from the NFC-grown 3D spheroids and keeping the spheroids in culture for long-term, we used it to compare EV production with spheroid growth and morphology by using optically transparent aNFC. The EV enumeration by NTA, spheroid morphology and size, the number of cells and protein content were analysed every two days for up to 11 days to determine the timeline of EV production and the optimal harvesting point in relation to the spheroid growth. On days 3, 5, 7, 9 and 11, the conditioned medium was harvested to isolate, quantitate, and characterize the secreted EVs without disturbing the spheroids (Figure 5A). According to the sequential measurements, the optimal growth time for the spheroids of A2058 melanoma cells was day 7, when the average spheroid area was 25.7 mm^2 $\pm$ 12.1 μm^2 (Figure 5A). However, based on the standard deviation, the spheroid sizes were very heterogeneous.

To enable comparison of the EV production with the spheroid growth in a time–dependent manner, we obtained the conditioned medium every two days, but this time without disturbing the spheroid cultures. From parallel wells, we also harvested the spheroids by enzymatic digestion to obtain individual cells for counting after trypsinization (Figure 5B) and to quantitate cellular total protein (Figure 5C). Next, we investigated the EV production (Figure 5D and Supplementary Figure 5) and counted the ratio of EVs/spheroid cell number (Figure 5E). The highest particle concentrations were detected between days 3 and 7 (Figure 5E). The best yield of EVs based on the particle concentration/cell was obtained on day 3 and 5. Based on the cell count and total
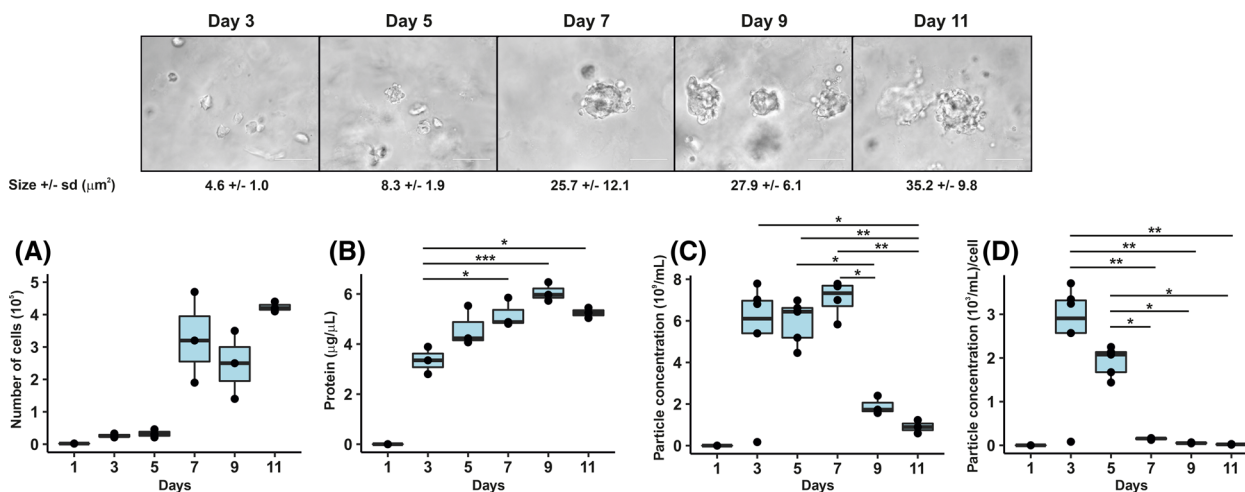
FIGURE 5 Comparison of EV production with spheroid growth, cell number and total protein. (A) Spheroids' live imaging shows the morphology and size when cultured up to 11 days in aNFC. (B) Number of cells within 3D A2058 melanoma spheroids followed up to 11 days from three independent experiments. (C) Total protein concentration of the 3D spheroids from three independent experiments. (D) Particle concentration of the isolated EV samples from the conditioned medium by NTA from 3 to 6 independent experiments. The spheroids were lysed using RIPA buffer and total protein concentration was determined by the Lowry method from three independent experiments. (E) EV production yield shown as ratio of particles/cell count. Statistics: ANOVA with Tukey's post-hoc test. (**) $P < 0.01$; (***) $P < 0.001$

protein, it could be determined that spheroid growth was stabilized by day 7, and further, also the EV production (measured by NTA – (NTA size-distribution graphics: Supplementary Figure 5)) peaked at day 7 and was then substantially decreased at days 9 and 11 (Figure 5E). Finally, it was observed that the two nanocellulose matrices, NFC and aNFC, used with the same cell line at the same concentrations (seeding & matrix) generated different production profiles and EV yields (Supplementary Figure 11).

3.4 | Characterization of the NFC 3D culture-derived extracellular vesicles

At the final stage of the current pipeline, EVs were isolated from the conditioned medium of MCF7 and A2058 cells by ultra-centrifugation and characterized by single particle interferometric reflectance imaging sensor (SP-IRIS), western blotting and transmission electron microscopy, according to the MISEV guidelines (Théry et al., 2018). Antibody staining of tetraspanins CD81, CD63 and CD9 of both EV types revealed abundant expression of all the tetraspanins (Figure 6). A2058 aNFC-grown EVs showed a change in the overall tetraspanin expression profile between days 3–5 and days 7–11. This difference was also seen in the profiles of CD63 and CD9 single labelled EVs (Supplementary Figure 6). The tetraspanin particle counts were similar between the A2058 EVs from day 5 and MCF7 from day 7. A2058 aNFC EVs from day 11 and A2058 ULA EVs from day 11 (Supplementary Figure 10) also displayed similar total particle counts based on tetraspanin binding to the respective antibody-coated chips.

Based on co-localization analysis of the three tetraspanins, some EVs were only positive for either CD81, CD63 or CD9 shown by single colour representation, but in the majority of the captured EVs, the tetraspanins were co-localized, (Supplementary Figure 6). The percentage of single labelled CD81 in A2058 aNFC derived EVs out of the total decreased from day 3 to day 11, and it was similar as in the EVs from the A2058 ULA on day 11 and from MCF7 NFC on day 7. The percentage of CD81 and CD9 double labelled EVs was similar in A2058 aNFC-derived EVs on day 7 and A2058 ULA on day 11. Percentage of the triple labelled (CD81, CD63 and CD9) particles was similar in all conditions, that is, A2058 aNFC day 11, MCF7 NFC day 7 and A2058 ULA day 11 (Supplementary Figure 6). In summary, despite the different methods and cell lines, the tetraspanin profiles were surprisingly alike at the analysis endpoints demonstrated by the similar percentage of the tetraspanin triple labelled particles. After SP-IRIS, western blot was performed to investigate cell-derived contamination in the EV samples using calnexin (cell marker) and CD9 as an EV marker (Supplementary Figure 7). Unlike the cell controls of A2058 spheroids, EVs from neither method were positive for calnexin, but were positive for CD9. In transmission electron microscopy, the detected EVs presented spherical morphology considered typical for EVs in EM ("cup-shape") and were heterogeneous in size (Supplementary Figure 8).

To show that the functionality of EVs prepared by harvesting and batch methods was the same despite the differences in the methodological steps during the isolation and thereby the robustness and usability of the methods in different laboratories, A2058 cell-derived EVs were prepared by both methods and co-cultured with human embryonic kidney cells (HEK293). More cells/frame were observed when EVs were added to the HEK293 cells in contrast to controls (no EVs or cellulase only), indicating that the EVs obtained by either method induced cell proliferation. There was no statistical difference between the harvest and the batch methods regarding the nuclei counts (Supplementary Figure 9C). The morphology of the HEK293 cells after the
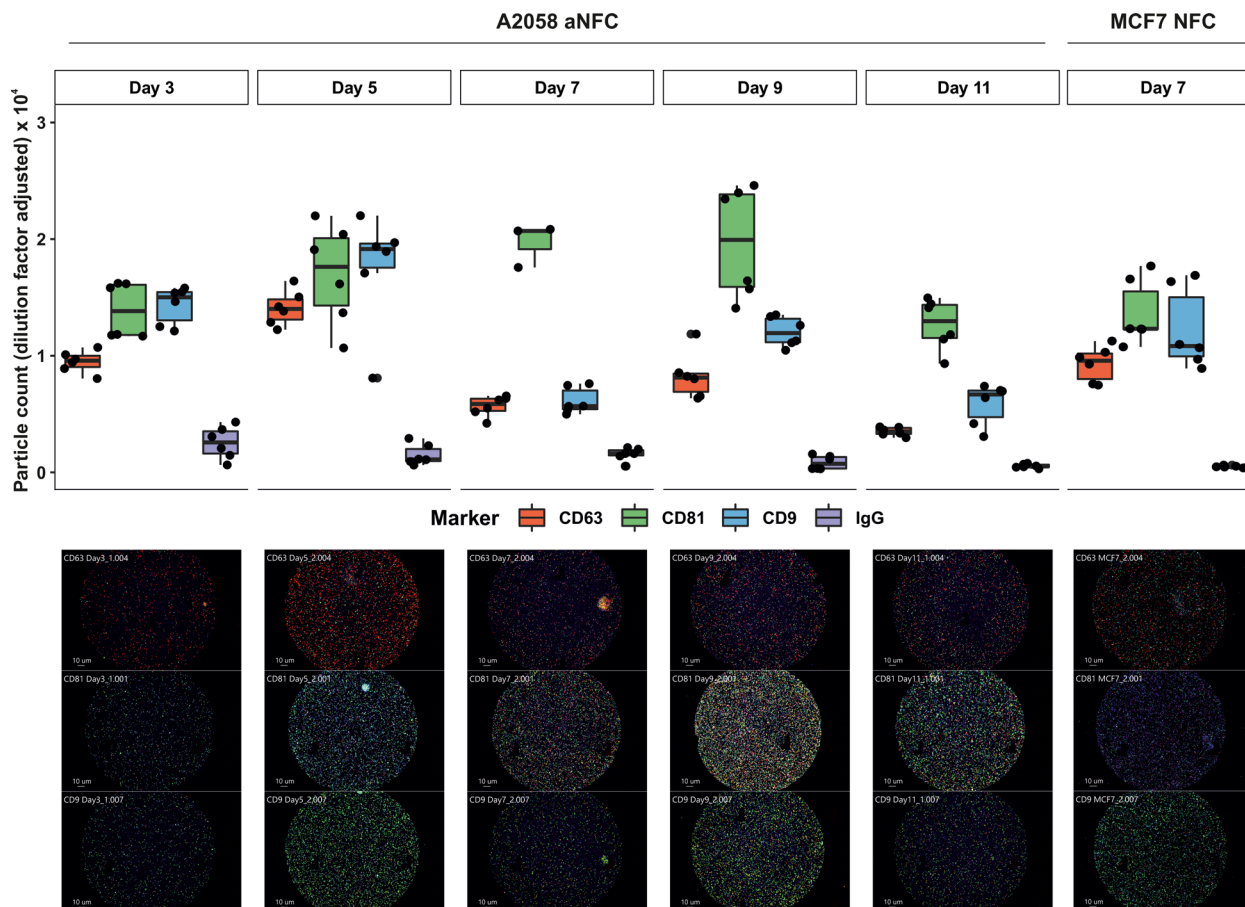
FIGURE 6 **EV characterization by SP-IRIS**. EV characterization by SP-IRIS from A2058 spheroids with harvesting method (days 3–11) and MCF7 spheroids with batch method (day 7) with secondary labelling of EVs on CD9, CD81 and CD63 antibody capture spots: anti-CD9 (488A – blue), anti-CD81 (555 – green), and anti-CD63 (647 – red). The boxplot shows the total particle count from the correspondent antibody-spot, and replicates are represented by dot plot. On the bottom of the graphics, fluorescence microscopy representative images of 3D-derived EVs measured. Particle count and size data is shown in Supplementary File T1 and T2

EV treatment showed a "fibroblast-like" morphology in the presence of EVs isolated with or without cellulase in contrast to a "spherical-like" morphology observed in the absence of EVs (control) or with the "cellulase only" – control (Supplementary Figure 9D).

3.5 | Comparison of 3D culture-derived EV production in NFC-scaffold and in a scaffold-free cultures

To compare the EV production from spheroids grown in NFC hydrogel scaffold with spheroid grown without matrix support, A2058 cells were seeded into ULA plates, which also enables the culture of single spheroids. The two platforms were compared to evaluate the feasibility of the NFC-use (Figure 4) in comparison to scaffold-free ULA-plates (Figure 7). Every other day for 11 days, EV production was evaluated by the particle number and size distributions by NTA (Figure 7 – (NTA size-distribution graphics: Supplementary Figure 10), and EV characterization was made by SP-IRIS (Supplementary Figure 11) and transmission electron microscopy (Supplementary Figure 8). On day 11, the number of cells and protein content were analysed to determine differences on spheroid growth between the methods, and no differences between the protein concentration and number of cells were noticed (Supplementary Table 3). Concerning the efficiency of scaffold-free spheroid generation, ULA plates generated 0.12×10^{10} EVs/well and 0.22×10^{10} EVs/well when the medium was either refreshed or topped up, respectively (Figure 7 and Supplementary Table 4). This suggests that the EV production efficiency by NFC was approximately 10-fold higher compared to the EV production by ULA plate (Supplementary Figure 12). Since the EV yield per cell was comparable between NFC and ULA plates (top-up) (Supplementary Table 4), and the EV marker expression was similar, albeit not identical (Supplementary Figure 6) between the two platforms, both the NFC and ULA platforms are compatible for EV production, and the differences are scalability and ease of operation enabling higher yield.
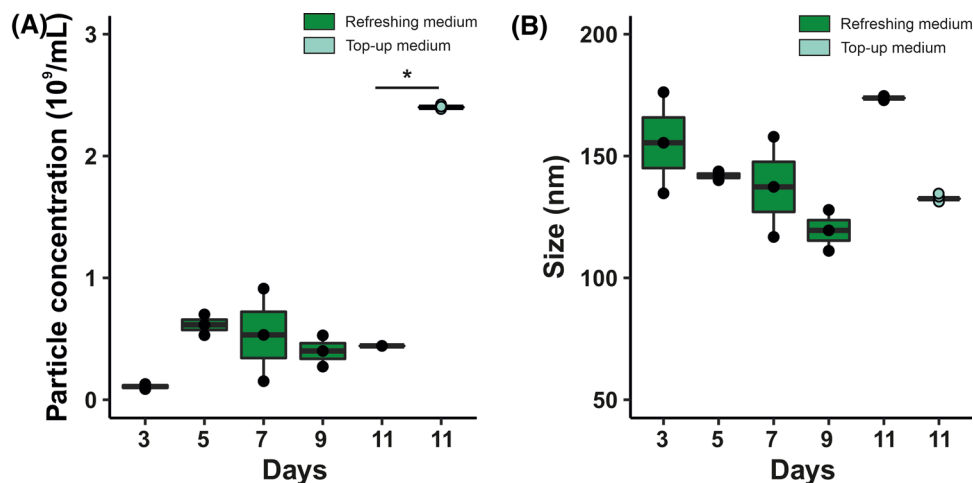
FIGURE 7 **EV production by the harvesting method using ULA plate**. Comparison between refreshing the medium completely and topping up with fresh medium. (A–B) A2058 cells were seeded in the ULA plate, and the conditioned medium was harvested for EV isolation, and particle concentration (A) and particle size (B) were measured by NTA from 3 independent experiments. Statistics: ANOVA with Tukey's post-hoc test. Day 11 top-up medium vs Day 11 refreshing medium: (*) $P < 0.05$

4 | DISCUSSION

The impact of generating in *vivo*-like conditions in cell culture is receiving increasing attention. Thus, the development and use of various 3D cell culture models has gained interest in different areas of cell biological research. The ability to provide more in *vivo*-like cell culture conditions and to mimic tissue structures and the extracellular environment by 3D spheroids is essential for studying both normal tissue behaviour and disease mechanisms. Additionally, the development of more complex 3D cultures can provide a useful middle ground between in *vitro* and in *vivo* experiments and help to decrease the need of animals in experiments. Critically in the EV field, recent studies comparing 2D and 3D culture -derived EVs have demonstrated culture condition –dependent impact in the EV properties including size (Rocha et al., 2018; Villasante et al., 2016), cargo (Palviainen et al., 2019, Millan et al., 2021; Rocha et al., 2018; Thippabhotla et al., 2019; Villasante et al., 2021), therapeutic potential (Cha et al., 2018), secretion efficiency (Palviainen et al., 2019; Millan et al., 2021; Rocha et al., 2018; Thippabhotla et al., 2019), and drug-delivery potential (Liang et al., 2019). Predominantly, the 3D cultures as a source of EVs have been seen to be beneficial when compared to 2D, but opposite findings exist (Kusuma et al., 2022). This highlights the importance of testing and applying an appropriate in *vitro* cell culture model for each EV research application, which requires setting up and optimizing novel models.

Recently, several studies have shown the efficiency of 3D cultures in EV production, but rarely with quantitative results. A prostate cell culture (PNT1A, LNCaP, PC3) in 3D chitosan-alginate hydrogel produced 300–800 EVs/cell (EV isolation by ultra-filtration and SEC), harvested after 4 days in culture (Millan et al., 2021). Spheroids of neuroblastoma cell line (SK-N-BE(2), LAI5s, SK-N-LP) grown in collagen I - hyaluronan matrix produced 0.6–1.3×10^8 EVs/ml (EV isolation by commercial kit) after 7 days in culture (Villasante et al., 2021). Furthermore, HeLa cells cultured in peptide hydrogel system produced 250–1500 EVs/cell during culture periods of 5–13 days (EV isolation by centrifugation and filtration) (Thippabhotla et al., 2019). The novel NFC tumour spheroid method developed and optimized in this study with human breast cancer (MCF7) and melanoma (A2058) cell lines yielded a maximum of 1.2–20×10^4 particles/cell, being more efficient than the other models discussed here. However, it should be noted that the available details of the other models are limited to allow direct comparisons reliably.

Although production of EVs was comparable between the NFC method and using the ULA plates (top-up), when the yields per cell were compared, the obtention of EVs with the NFC method was much easier and more efficient than using the ULA plates regarding both labour and time: ten ULA wells were needed to obtain the same amount of EVs as from a well of NFC culture. As of now, there is a severe lack of knowledge of the impact of different 3D culture methods on EV production and properties. From the point of view of the different cell biological determinants (adhesion, growth pattern, matrix properties and cell-cell interaction), the "floating" of cells in the ULA plates may impact spheroid growth differently from the matrix-based interactions amendable to the spheroids grown in NFC. The fibrillary NFC mimics the ECM structure, and cells grow as single-cell spheroids. In contrast, the scaffold-free ULA plate lacks the adhesive/adherent structures and the spheroids growth as aggregates. These differences may interfere with cell behaviour and growth (Coleman et al., 2007; Jensen & Teng, 2020; Habanjar et al., 2021), and consequently, the EV profile. Based on our data, changes in CD81 and CD9 expression were observed when comparing the EVs from the A2058 aNFC and ULA spheroids. Therefore, future studies should focus on elucidating the impact of the used 3D culture method and growth conditions on EV properties.

We found the NFC hydrogel to be a promising 3D culture scaffold option for spheroid cultures and for efficient isolation of 3D cell culture-derived EVs. As a well-defined and animal-free matrix, NFC provides an alternative for biological scaffolds, shown to also suffer from batch-to-batch variability (Hughes et al., 2010) affecting the reproducibility of the experiments. In some cases, biological scaffolds can also contain matrix bound vesicles (Huleihel et al., 2016). Generally, NFC materials induce minimal cytotoxic effects on cells (Athinarayanan et al., 2018; Li et al., 2021; Nordli et al., 2016), although the cytotoxicity of nanocellulose might be dependent on its length (Li et al., 2021). Furthermore, cellulase digestion was shown to be unharmful to animal cells (Lou et al., 2014). We observed high viability and no necrotic core formation in both cell lines up to 11 days of culture. Additionally, the grown spheroids showcased cell type -specific morphologies, such as lumen-like structure formation of epithelial luminal MCF7 cell line, as previously seen when grown in animal-based matrices (Krause et al., 2010).

Tuneable scaffold viscosity allows modelling of different growth environments and could be adjusted to support the growth of different cell types. It is worth noting though, that the growth conditions, including the used NFC concentration, must be individually optimized for each cell line. Accordingly, we also observed a difference between NFC and aNFC scaffolds in the EV yield and time course, independent of the same culture conditions, which may implicate preferential chemical properties of aNFC or differences in matrix stiffness. Both matrices are nanocellulose, but NFC is a native sugar, while aNFC is anionic (Na$^+$ salt – 20% of the hydroxyl groups ionized) (Koivuniemi et al., 2021). With shorter and thinner fibres (Sheard et al., 2019), aNFC is more viscous than NFC at 0.5% concentration, which may have an impact to, for example, cell proliferation and thereby the EV production. In addition to its biocompatibility, the improved optical properties of aNFC make it compatible with imaging, as NFC does not emit autofluorescence (Sheard et al., 2019) making it ideal also for imaging 3D cultures. A challenge in isolating EVs from a scaffold-based method is the remaining particles from digested hydrogels, which may interfere with the EV isolation or purity of the final sample. To circumvent this, we provide here two complementary approaches: one, in which the EV isolation is performed from a cellulase-digested scaffold and another without digestion performed by collecting the conditioned medium for EV isolation and replating the tumour spheroid & NFC into the culture with refreshed medium.

5 | CONCLUSION

In conclusion, we have established a pipeline for an easy, quick, and tuneable isolation of EVs from 3D spheroids grown in NFC scaffold. NFC provides a mouldable and reproducible platform for spheroid growth and importantly supports efficient secretion of EVs from cancer cells, which can be adapted for different cell lines and EV isolation methods. The two created methods provide (i) maximal yield of EVs as a batch isolation at the end of spheroid growth or (ii) access to comparison of EV production with spheroid growth and spheroid morphology by a time-dependent successive harvesting of EVs during continuous culture. The latter method could be tailored, for example for drug-delivery studies or analysing the impact of cell culture conditions, for example, hypoxia or cell treatments in EV productions. Together, the two methods offer tuneable access to 3D cell cultured EVs providing opportunities for elucidating the basic biology of EVs, preclinical applications such as drug testing, and for developing EV-based biomaterials.

CONFLICT OF INTERESTS
GrowDex®, GrowDex®-T and GrowDase™ were received from UPM Biomedicals as an in-kind contribution to their participation in the EVE consortium funded by Business Finland.

AUTHOR CONTRIBUTIONS
Heikki Kyykallio: Formal analysis; Methodology; Writing – original draft. Alessandra V.S. Faria: Formal analysis; Methodology; Writing – original draft. Rosabella Hartmann: Methodology. Janne Capra: Methodology; Supervision. Kirsi Rilla: Funding acquisition; Supervision; Writing – review & editing. Pia R-M Siljander: Funding acquisition; Supervision; Writing – review & editing.

ORCID
Heikki Kyykallio https://orcid.org/0000-0002-8455-876X
Alessandra V. S. Faria https://orcid.org/0000-0003-1161-5724
Kirsi Rilla https://orcid.org/0000-0002-7862-5727
Pia R-M Siljander https://orcid.org/0000-0003-2326-5821

REFERENCES

Abdollahi, S. (2021). Extracellular vesicles from organoids and 3D culture systems. *Biotechnology and Bioengineering*, *118*(3), 1029–1049. https://doi.org/10.1002/bit.27606

Athinarayanan, J., Periasamy, V. S., & Alshatwi, A. A. (2018). Fabrication and cytotoxicity assessment of cellulose nanofibrils using Bassia eriophora biomass. *International Journal of Biological Macromolecules*, *117*, 911–918. https://doi.org/10.1016/j.ijbiomac.2018.05.144

Azoidis, I., Metcalfe, J., Reynolds, J., Keeton, S., Hakki, S., Sheard, J., & Widera, D. (2017). Three-dimensional cell culture of human mesenchymal stem cells in nanofibrillar cellulose hydrogels. *MRS Communications*, *7*(3), 458–465. https://doi.org/10.1557/mrc.2017.59

Benton, G., Arnaoutova, I., George, J., Kleinman, H. K., & Koblinski, J. (2014). Matrigel: From discovery and ECM mimicry to assays and models for cancer research. *Advanced Drug Delivery Reviews*, *79–80*, 3–18. https://doi.org/10.1016/j.addr.2014.06.005

Bhattacharya, M., Malinen, M. M., Lauren, P., Lou, Y. R., Kuisma, S. W., Kanninen, L., Lille, M., Corlu, A., GuGuen-Guillouzo, C., Ikkala, O., Laukkanen, A., Urtti, A., & Yliperttula, M. (2012). Nanofibrillar cellulose hydrogel promotes three-dimensional liver cell culture. *Journal of Controlled Release: Official Journal of the Controlled Release Society*, *164*(3), 291–298. https://doi.org/10.1016/j.jconrel.2012.06.039

Bicer, M., Sheard, J., Iandolo, D., Boateng, S. Y., Cottrell, G. S., & Widera, D. (2020). Electrical stimulation of adipose-derived stem cells in 3D nanofibrillar cellulose increases their osteogenic potential. *Biomolecules*, *10*(12), 1–18. https://doi.org/10.3390/biom10121696

Caliari, S. R., & Burdick, J. A. (2016). A practical guide to hydrogels for cell culture. *Nature Methods*, *13*(5), 405–414. https://doi.org/10.1038/nmeth.3839

Cha, J. M., Shin, E. K., Sung, J. H., Moon, G. J., Kim, E. H., Cho, Y. H., Park, H. D., Bae, H., Kim, J., & Bang, O. Y. (2018). Efficient scalable production of therapeutic microvesicles derived from human mesenchymal stem cells. *Scientific Reports*, *8*(1), 1171. https://doi.org/10.1038/s41598-018-19211-6

Coleman, C. B., Gonzalez-Villalobos, R. A., Allen, P. L., Johanson, K., Guevorkian, K., Valles, J. M., & Hammond, T. G. (2007). Diamagnetic levitation changes growth, cell cycle, and gene expression of Saccharomyces cerevisiae. *Biotechnology and Bioengineering*, *98*(4), 854–863. https://doi.org/10.1002/bit.21526

Curvello, R., Raghuwanshi, V. S., & Garnier, G. (2019). Engineering nanocellulose hydrogels for biomedical applications. *Advances in Colloid and Interface Science*, *267*, 47–61. https://doi.org/10.1016/j.cis.2019.03.002

Duval, K., Grover, H., Han, L. H., Mou, Y., Pegoraro, A. F., Fredberg, J., & Chen, Z. (2017). Modeling physiological events in 2D vs. *3D Cell Culture. Physiology (Bethesda, Md.)*, *32*(4), 266–277. https://doi.org/10.1152/physiol.00036.2016

Edmondson, R., Broglie, J. J., Adcock, A. F., & Yang, L. (2014). Three-dimensional cell culture systems and their applications in drug discovery and cell-based biosensors. *Assay and Drug Development Technologies*, *12*(4), 207–218. https://doi.org/10.1089/adt.2014.573

Faria, A., Clerici, S. P., de Souza Oliveira, P. F., Queiroz, K., Peppelenbosch, M. P., & Ferreira-Halder, C. V. (2020). LMWPTP modulates the antioxidant response and autophagy process in human chronic myeloid leukemia cells. *Molecular and Cellular Biochemistry*, *466*(1–2), 83–89. https://doi.org/10.1007/s11010-020-03690-1

Gudbergsson, J. M., Johnsen, K. B., Skov, M. N., & Duroux, M. (2016). Systematic review of factors influencing extracellular vesicle yield from cell cultures. *Cytotechnology*, *68*(4), 579–592. https://doi.org/10.1007/s10616-015-9913-6

Habanjar, O., Diab-Assaf, M., Caldefie-Chezet, F., & Delort, L. (2021). 3D cell culture systems: Tumor application, advantages, and disadvantages. *International Journal of Molecular Sciences*, *22*(22), 12200. https://doi.org/10.3390/ijms222212200

Hughes, C. S., Postovit, L. M., & Lajoie, G. A. (2010). Matrigel: A complex protein mixture required for optimal growth of cell culture. *Proteomics*, *10*(9), 1886–1890. https://doi.org/10.1002/pmic.200900758

Huleihel, L., Hussey, G. S., Naranjo, J. D., Zhang, L., Dziki, J. L., Turner, N. J., Stolz, D. B., & Badylak, S. F. (2016). Matrix-bound nanovesicles within ECM bioscaffolds. *Science Advances*, *2*(6), 1600502. https://doi.org/10.1126/sciadv.1600502

Jensen, C., & Teng, Y. (2020). Is it time to start transitioning from 2D to 3D cell culture? *Frontiers in Molecular Biosciences*, *7*, 33. https://doi.org/10.3389/fmolb.2020.00033

Koivuniemi, R., Xu, Q., Snirvi, J., Lara-Sáez, I., Merivaara, A., Luukko, K., Nuopponen, M., Wang, W., & Yliperttula, M. (2021). Comparison of the therapeutic effects of native and anionic nanofibrillar cellulose hydrogels for full-thickness skin wound healing. *Micro*, *1*(2), 194–214. https://doi.org/10.3390/micro1020015

Krause, S., Maffini, M. V., Soto, A. M., & Sonnenschein, C. (2010). The microenvironment determines the breast cancer cells' phenotype: Organization of MCF7 cells in 3D cultures. *BMC Cancer*, *10*, 263. https://doi.org/10.1186/1471-2407-10-263

Kusuma, G. D., Li, A., Zhu, D., McDonald, H., Inocencio, I. M., Chambers, D. C., Sinclair, K., Fang, H., Greening, D. W., Frith, J. E., & Lim, R. (2022). Effect of 2D and 3D culture microenvironments on mesenchymal stem cell-derived extracellular vesicles potencies. *Frontiers in Cell and Developmental Biology*, *10*, 819726. https://doi.org/10.3389/fcell.2022.819726

Laukkanen, K., Saarinen, M., Mallet, F., Aatonen, M., Hau, A., & Ranki, A. (2020). Cutaneous T-cell lymphoma (CTCL) cell line-derived extracellular vesicles contain HERV-W-encoded fusogenic syncytin-1. *The Journal of Investigative Dermatology*, *140*(7), 1466–1469.e4. https://doi.org/10.1016/j.jid.2019.11.021

Li, J., Wang, X., Chang, C. H., Jiang, J., Liu, Q., Liu, X., Liao, Y.-P., Ma, T., Meng, H., & Xia, T. (2021). Nanocellulose length determines the differential cytotoxic effects and inflammatory responses in macrophages and hepatocytes. *Small*, 2102545. https://doi.org/10.1002/SMLL.202102545

Liang, Q., Bie, N., Yong, T., Tang, K., Shi, X., Wei, Z., Jia, H., Zhang, X., Zhao, H., Huang, W., Gan, L., Huang, B., & Yang, X. (2019). The softness of tumour-cell-derived microparticles regulates their drug-delivery efficiency. *Nature Biomedical Engineering*, *3*(9), 729–740. https://doi.org/10.1038/s41551-019-0405-4

Lou, Y.-R., Kanninen, L., Kuisma, T., Niklander, J., Noon, L. A., Burks, D., Urtti, A., & Yliperttula, M. (2014). The use of nanofibrillar cellulose hydrogel as a flexible three-dimensional model to culture human pluripotent stem cells. *Stem Cells and Development*, *23*(4), 380. https://doi.org/10.1089/SCD.2013.0314

Malinen, M. M., Kanninen, L. K., Corlu, A., Isoniemi, H. M., Lou, Y. R., Yliperttula, M. L., & Urtti, A. O. (2014). Differentiation of liver progenitor cell line to functional organotypic cultures in 3D nanofibrillar cellulose and hyaluronan-gelatin hydrogels. *Biomaterials*, *35*(19), 5110–5121. https://doi.org/10.1016/j.biomaterials.2014.03.020

Millan, C., Prause, L., Vallmajo-Martin, Q., Hensky, N., & Eberli, D. (2021). Extracellular vesicles from 3D engineered microtissues harbor disease-related cargo absent in EVs from 2D cultures. Advanced healthcare materials, e2002067. Advance online publication. https://doi.org/10.1002/adhm.202002067

Mäkelä, R., Arjonen, A., Härmä, V., Rintanen, N., Paasonen, L., Paprotka, T., Rönsch, K., Kuopio, T., Kononen, J., & Rantala, J. K. (2020). Ex vivo modelling of drug efficacy in a rare metastatic urachal carcinoma. *BMC Cancer*, *20*(1), 590. https://doi.org/10.1186/s12885-020-07092-w

Nath, S., & Devi, G. R. (2016). Three-dimensional culture systems in cancer research: focus on tumor spheroid model. *Pharmacology & Therapeutics*, *163*, 94. https://doi.org/10.1016/J.PHARMTHERA.2016.03.013

Nguyen, V., Witwer, K. W., Verhaar, M. C., Strunk, D., & van Balkom, B. (2020). Functional assays to assess the therapeutic potential of extracellular vesicles. *Journal of Extracellular Vesicles*, *10*(1), e12033. https://doi.org/10.1002/jev2.12033

Nordli, H. R., Chinga-Carrasco, G., Rokstad, A. M., & Pukstad, B. (2016). Producing ultrapure wood cellulose nanofibrils and evaluating the cytotoxicity using human skin cells. *Carbohydrate Polymers*, *150*, 65–73. https://doi.org/10.1016/j.carbpol.2016.04.094

Pacienza, N., Lee, R. H., Bae, E. H., Kim, D. K., Liu, Q., Prockop, D. J., & Yannarelli, G. (2018). In vitro macrophage assay predicts the in vivo anti-inflammatory potential of exosomes from human mesenchymal stromal cells. Molecular therapy. *Methods & Clinical Development*, *13*, 67–76. https://doi.org/10.1016/j.omtm.2018.12.003

Palviainen, M., Saari, H., Kärkkäinen, O., Pekkinen, J., Auriola, S., Yliperttula, M., Puhka, M., Hanhineva, K., & Siljander, P. R. (2019). Metabolic signature of extracellular vesicles depends on the cell culture conditions. *Journal of Extracellular Vesicles*, *8*(1), 1596669. https://doi.org/10.1080/20013078.2019.1596669

Palviainen, M., Laukkanen, K., Tavukcuoglu, Z., Velagapudi, V., Kärkkäinen, O., Hanhineva, K., Auriola, S., Ranki, A., & Siljander, P. (2020). Cancer alters the metabolic fingerprint of extracellular vesicles. *Cancers*, *12*(11), 3292. https://doi.org/10.3390/cancers12113292

Puhka, M., Nordberg, M. E., Valkonen, S., Rannikko, A., Kallioniemi, O., Siljander, P., & Hällström, A, T, M. (2017). KeepEX, a simple dilution protocol for improving extracellular vesicle yields from urine. *European Journal of Pharmaceutical Sciences: Official Journal of the European Federation for Pharmaceutical Sciences*, *98*, 30–39. https://doi.org/10.1016/j.ejps.2016.10.021

Pääkkö, M., Ankerfors, M., Kosonen, H., Nykänen, A., Ahola, S., Osterberg, M., Ruokolainen, J., Laine, J., Larsson, P. T., Ikkala, O., & Lindström, T. (2007). Enzymatic hydrolysis combined with mechanical shearing and high-pressure homogenization for nanoscale cellulose fibrils and strong gels. *Biomacromolecules*, *8*(6), 1934–1941. https://doi.org/10.1021/bm061215p

R Core Team (2013). *R: A language and environment for statistical computing*. R Foundation for Statistical Computing. URL https://www.R-project.org/

Rinner, B., Gandolfi, G., Meditz, K., Frisch, M. T., Wagner, K., Ciarrocchi, A., Torricelli, F., Koivuniemi, R., Niklander, J., Liegl-Atzwanger, B., Lohberger, B., Heitzer, E., Ghaffari-Tabrizi-Wizsy, N., Zweytick, D., & Zalaudek, I. (2017). MUG-Mel2, a novel highly pigmented and well characterized NRAS mutated human melanoma cell line. *Scientific Reports*, *7*(1), 2098. https://doi.org/10.1038/s41598-017-02197-y

Rocha, S., Carvalho, J., Oliveira, P., Voglstaetter, M., Schvartz, D., Thomsen, A. R., Walter, N., Khanduri, R., Sanchez, J. C., Keller, A., Oliveira, C., & Nazarenko, I. (2018). 3D cellular architecture affects microRNA and protein cargo of extracellular vesicles. *Advanced Science (Weinheim, Baden-Wurttemberg, Germany)*, *6*(4), 1800948. https://doi.org/10.1002/advs.201800948

Sadovska, L., Zandberga, E., Sagini, K., Jēkabsons, K., Riekstiņa, U., Kalniņa, Z., Llorente, A., & Linē, A. (2018). A novel 3D heterotypic spheroid model for studying extracellular vesicle-mediated tumour and immune cell communication. *Biochemical and Biophysical Research Communications*, *495*(2), 1930–1935. https://doi.org/10.1016/j.bbrc.2017.12.072

Schindelin, J., Arganda-Carreras, I., Frise, E., Kaynig, V., Longair, M., Pietzsch, T., Preibisch, S., Rueden, C., Saalfeld, S., Schmid, B., Tinevez, J. Y., White, D. J., Hartenstein, V., Eliceiri, K., Tomancak, P., & Cardona, A. (2012). Fiji: An open-source platform for biological-image analysis. *Nature Methods*, *9*(7), 676–682. https://doi.org/10.1038/nmeth.2019

Sheard, J. J., Bicer, M., Meng, Y., Frigo, A., Aguilar, R. M., Vallance, T. M., Iandolo, D., & Widera, D. (2019). Optically transparent anionic nanofibrillar cellulose is cytocompatible with human adipose tissue-derived stem cells and allows simple imaging in 3D. *Stem Cells International*, 2019. https://doi.org/10.1155/2019/3106929

Siiskonen, H., Rilla, K., Kärnä, R., Bart, G., Jing, W., Haller, M. F., DeAngelis, P. L., Tammi, R. H., & Tammi, M. I. (2013). Hyaluronan in cytosol–microinjection-based probing of its existence and suggested functions. *Glycobiology*, *23*(2), 222–231. https://doi.org/10.1093/glycob/cws149

Thippabhotla, S., Zhong, C., & He, M. (2019). 3D cell culture stimulates the secretion of in vivo like extracellular vesicles. *Scientific Reports*, *9*(1), 13012. https://doi.org/10.1038/s41598-019-49671-3

Théry, C., Witwer, K. W., Aikawa, E., Alcaraz, M. J., Anderson, J. D., Andriantsitohaina, R., Antoniou, A., Arab, T., Archer, F., Atkin-Smith, G. K., Ayre, D. C., Bach, J. M., Bachurski, D., Baharvand, H., Balaj, L., Baldacchino, S., Bauer, N. N., Baxter, A. A., Bebawy, M., … Zuba-Surma, E. K. (2018). Minimal information for studies of extracellular vesicles 2018 (MISEV2018): A position statement of the International Society for Extracellular Vesicles and update of the MISEV2014 guidelines. *Journal of Extracellular Vesicles*, *7*(1). https://doi.org/10.1080/20013078.2018.1535750

Toivonen, S., Malinen, M. M., Küblbeck, J., Petsalo, A., Urtti, A., Honkakoski, P., & Otonkoski, T. (2016). Regulation of human pluripotent stem cell-derived hepatic cell phenotype by three-dimensional hydrogel models. *Tissue Engineering - Part A*, *22*(13–14), 971–984. https://doi.org/10.1089/ten.tea.2016.0127

Vidi, P. A., Bissell, M. J., & Lelièvre, S. A. (2013). Three-dimensional culture of human breast epithelial cells: The how and the why. *Methods in Molecular Biology (Clifton, N.J.)*, *945*, 193–219. https://doi.org/10.1007/978-1-62703-125-7_13

Villasante, A., Godier-Furnemont, A., Hernandez-Barranco, A., Coq, J. L., Boskovic, J., Peinado, H., Mora, J., Samitier, J., & Vunjak-Novakovic, G. (2021). Horizontal transfer of the stemness-related markers EZH2 and GLI1 by neuroblastoma-derived extracellular vesicles in stromal cells. *Translational Research: The Journal of Laboratory and Clinical Medicine*, *237*, 82–97. https://doi.org/10.1016/j.trsl.2021.06.006

Villasante, A., Marturano-Kruik, A., Ambati, S. R., Liu, Z., Godier-Furnemont, A., Parsa, H., Lee, B. W., Moore, M. A., & Vunjak-Novakovic, G. (2016). Recapitulating the size and cargo of tumor exosomes in a tissue-engineered model. *Theranostics*, *6*(8), 1119–1130. https://doi.org/10.7150/thno.13944

Xie, L., Mao, M., Zhou, L., Zhang, L., & Jiang, B. (2017). Signal factors secreted by 2D and spheroid mesenchymal stem cells and by cocultures of mesenchymal stem cells derived microvesicles and retinal photoreceptor neurons. *Stem Cells International*, *2017*, 2730472–13. https://doi.org/10.1155/2017/2730472

Yang, Y., Knight, R., Stephens, P., & Zhang, Y. (2020). Three-dimensional culture of oral progenitor cells: Effects on small extracellular vesicles production and proliferative function. *Journal of Oral Pathology & Medicine*, *49*(4), 342–349. https://doi.org/10.1111/jop.12981

Zhang, Y., Chopp, M., Zhang, Z. G., Katakowski, M., Xin, H., Qu, C., Ali, M., Mahmood, A., & Xiong, Y. (2017). Systemic administration of cell-free exosomes generated by human bone marrow derived mesenchymal stem cells cultured under 2D and 3D conditions improves functional recovery in rats after traumatic brain injury. *Neurochemistry International*, *111*, 69–81. https://doi.org/10.1016/j.neuint.2016.08.003

SUPPORTING INFORMATION

Additional supporting information can be found online in the Supporting Information section at the end of this article.